

Blow-off characteristics of turbulent premixed flames in curved-wall Jet Burner

Morkous S. Mansour^{1,2}, O. Mannaa¹, S. K. Chung¹

¹Clean Combustion Research Centre, King Abdullah University of Science and Technology, Thuwal, Saudi Arabia

²Department of Mechanical Engineering, Helwan University, Cairo, Egypt

1 Abstract

This study concerns the flame dynamics of a curved-wall jet (CWJ) stabilized turbulent premixed flame as it approaches blow-off conditions. Time resolved OH planar laser-induced fluorescence (PLIF) delineated reaction zone contours and simultaneously stereoscopic particle image velocimetry (SPIV) quantified the turbulent flow field features. Ethylene/air flames were stabilized in CWJ burner to determine the sequence of events leading to blowoff. For stably burning flames far from blowoff, flames are characterized with a recirculation zone (RZ) upstream for flame stabilization followed by an intense turbulent interaction jet (IJ) and merged-jet regions downstream; the flame front counterparts the shear layer vortices. Near blowoff, as the velocity of reactants increases, high local stretch rates exceed the extinction stretch rates instantaneously resulting in localized flame extinction along the IJ region. As Reynolds number (Re) increases, flames become shorter and are entrained by larger amounts of cold reactants. The increased strain rates together with heat loss effects result in further fragmentation of the flame, eventually leading to the complete quenching of the flame. This is explained in terms of local turbulent Karlovitz stretch factor (K) and principal flow strain rates associated with \bar{C} contours. Hydrogen addition and increasing the RZ size lessen the tendency of flames to be locally extinguished.

2 Introduction

Stabilization of turbulent premixed flames, particularly for high-velocity flows, has been an important subject for combustion research over the past several decades for a variety of applications, such as in gas turbine combustors, afterburners, and industrial furnaces. Flame stabilization is frequently achieved by inducing a recirculation zone, where mixing of hot burned gases and radicals with fresh combustible gases could occur by providing long residence time. Bluff body [1], swirl [2], or jet-induced recirculating flows [3] are common practices. In this regard, Gil et al. [4] proposed a new type of burner, the ‘curved wall-jet (CWJ) burner’, to stabilize turbulent premixed flames exhibiting good stabilization characteristics. The burner utilized the Coanda effect [5], as schematically shown in Fig. 1a. In the turbulent premixed flame study [4], a mixture of fuel/air was injected over a curved wall as a form of annular-inward jet. Due to curvature of the streamlines, a low-pressure region was generated, resulting in flow adherence to the curved surface. As the static pressure recovers, the wall-jet is separated to form a recirculation zone (RZ). The annular-inward jet collides over the RZ in an interaction jet region, promoting the level of turbulence by the effect of collision and ambient air

entrainment, and subsequently develops as a merged jet in the downstream. Such burner resulted in improved flame stabilization and a short flame length. Kim et al. [6] further improved flame stabilization by modifying the burner tip, introducing a concave cavity on the tip.

Flame stabilization characteristics were investigated in a number of seminal works [7]. The flame blowoff criterion was recognized, and the effects of different bluff-body geometries on flame stabilization were identified. Lean blowoff limits were considered for different combustible mixtures, flame holder geometries, and variable thermodynamic conditions. Longwell [7] suggested that blowoff occurs as the rate of entrainment of reactants into the recirculation zone differs from the rate of burning of these reactants. Another mechanism is that the contact time between the combustible mixture and hot gases in the shear layer is not sufficiently enough compared with a chemical ignition time. Several studies have proposed alternative mechanisms based upon the local extinction by excessive flame stretch. However, the details of the blowoff mechanism associated with the flame dynamics just prior to blowoff still remain elusive.

In this study, we first discuss far and near blow-off characteristics of CWJ-burner turbulent premixed flames. The effect of the RZ size on such characteristics is investigated using two different burner tip configurations. Also, the effect of hydrogen addition is scrutinized to investigate any alterations imposed on these characteristics. Simultaneous high speed OH-PLIF and SPIV measurements were conducted and the analysis of these data in the near and far field of flame-anchoring region are presented to provide a detailed description of the flow field and flame structure respectively.

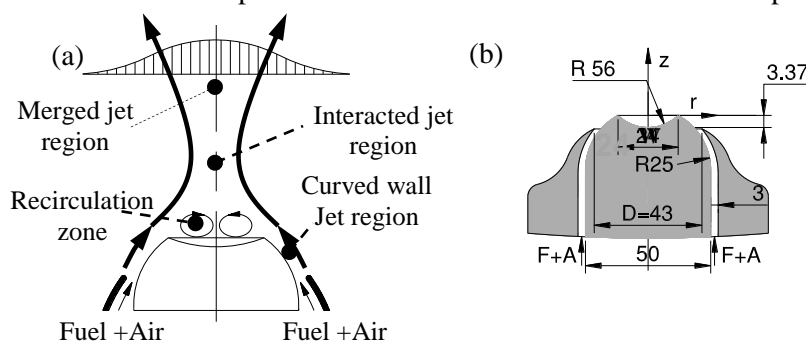


Figure. 1 Schematic of flow field in CWJ burner (a) CWJ-burner with dimensions (b).

3 Experiment

3.1 Burner system

The CWJ burner (Fig. 1b) is composed of an inner cylinder with 50 mm in diameter, having a hemispherical end. On the top, a concave cavity has a width (W) of 28 mm, a depth of 3.37 mm and $R = 56$ mm. Another concave cavity of 16 mm width was utilized to investigate its effect on the blowoff characteristics. An outer flow guide has a concentric cylinder with 56 mm i.d. with a converging section at the end having an exit diameter of 43 mm and $R = 25$ mm. The slit height between the hemisphere and the tip of the outer cylinder can be controlled and kept fixed in the present study at 0.5 mm. A further detailed description can be found in [4, 6].

Pre-mixtures of ethylene (>99.995%) and air were supplied through the slit and their flow rates were metered using mass flow controllers. Details of test conditions are listed in Table 1. The calculated Reynolds number, $Re = V_o D_e / \nu$, is based on the mean jet velocity, V_o , the kinematic viscosity of the mixture, ν , [8] and the effective diameter, $D_e = \sqrt{4A/\pi}$; V_o is defined as V_j/A , where V_j is the volume flow rate and A is the exit area at the slit, which is calculated from the normal projection from the tip of the inner cylinder to the center body. The exit area was kept constant at 65 mm^2 in the present study and V_o ranges from 24.5 to 78.7 m/s corresponding to Re of 15000 to 48200, respectively.

3.2 Stereoscopic PIV system

The SPIV system (La Vision, LDY 300) consisted of a high-repetition rate (up to 10 kHz) twin-cavity diode-pumped Nd: YLF laser (Litron, LDY304-PIV at 527 nm, 28 mJ/pulse, 5 ns pulse duration) and two CMOS cameras (La Vision, Imager Pro HS 4M with 2016×2016 pixels) coupled with a high

speed controller. The laser output is formed into a sheet using a two-lens cylindrical telescope and time separation of 10 to 40 μs are repeated at 3 kHz, producing a 3D vector field every 333 μs . Seed particles were TiO_2 having 0.18 μm nominal diameter. The Mie scattered light from each laser pulse is recorded on a separate frame. The two cameras were placed equidistant from, and on the same side of, the laser sheet to collect forward and backward scattered light at an angle of 45° with the laser sheet plane. Scheimpflug joining the lens to the camera had an angle of $5\text{-}7^\circ$ to project the focus plane to the target frame. A perspective distortion from the camera system was calibrated by imaging a 3-D dot target (Lavision type 11), which was also used to align the field of view from SPIV cameras with that from the OH-PLIF camera. The velocity vector fields were determined through multi-pass vector computation technique (Lavision Davis 8.1 software) with interrogation region size of 24×24 pixels having 50% overlap, equivalent to a spatial resolution of 0.85×0.85 mm. The system was operated at 3 kHz by recording 0.16 s duration such that 500 double-frame images were analyzed.

Table 1: Experimental conditions of investigated flames.

Flame	E1	E2	E3	E4	E5	E6
ϕ	1.0	1.0	1.0	1.2	0.9	0.9
V_o	24.5	52.7	78.7	52.7	44.1	44.1
$\text{Re} \times 10^3$	15	32.3	48.2	33	27.1	27.1
$\text{H}_2[\%]$	0	0	0	0	0	10

3.3 High speed OH-PLIF system

The fluorescence from OH radicals, as a flame front marker, was measured with the high-speed (up to 10 kHz) PLIF system. The system consisted of a frequency-doubled, diode-pumped solid state Nd:YAG laser (Edgewave, IS16II-E) that pumped a dye laser (Sirah, Credo-Dye). The dye was Rhodamine 6G in ethanol (0.09 g/L concentration). The output of the dye laser was frequency doubled to UV using BBO crystal and then tuned to excite the $Q_1(8)$ line of the A-X (1,0) OH transition at 283.57 nm with output energy of about 300 $\mu\text{J}/\text{pulse}$ at 10 kHz repetition rate. The UV laser beam was expanded through a two-lens cylindrical telescope configuration to form a collimated sheet of 70 mm in height at the target.

The fluorescence signals of OH at 295-345 nm were captured at a right angle to the laser sheet with an intensified CMOS camera (Lavision, HSS8 and IRO) with 1024×1024 pixels. Elastic scattering noise from the laser sheet and background luminosity were reduced by using a high-transmission band-pass interference filter ($>80\%$ at 320 nm) and also by minimizing the intensifier gate time (200 ns). Spatial resolution was about 0.11 mm/pixel.

3 Results and discussion

3.1 Flame structure and Blow-off characteristics

The instantaneous images of OH shown in Fig. 2 for flames E1-E3 reveal the existence of a recirculation zone upstream at the concave cavity followed by, for high Re flames, a thin neck at the interaction jet region and then the highest OH signal zone further downstream. By inspecting these images, we can derive the following features: (1) the RZ is fairly clear and confined within the burner tip for flames E2 and E3 as the velocity of recirculated gases increases with Re; (2) the production of OH radical in the interaction jet region is appreciably influenced in high Re flames (E2 and E3) where OH intensity is low while a broadening zone of relatively higher OH intensity is observed in flame E1; (3) the wrinkled reaction sheets distribute predominantly along the shear layers in low Re flames (E1), however, in high Re flames (E2 and E3), distributed reactions zones appear further downstream in a form of isolated islands associated with the abundance of OH species; such trend is more manifested in flame E3; (4) these images imply that the downstream part of the flame front is maintained by small flame elements detached from RZ, and its wrinkleness depends on the nature of flame seeds, emerging from the RZ.

Frequent events of local flame extinction are observed at the interaction jet region which is confirmed by conducting horizontal laser sheet measurements. Some flame kernels that initiated in the recirculation zone are detached at the interaction jet region and convected downstream toward the merged-jet region. As they encounter a favorable combustion environment, these kernels induce a re-ignition process further downstream as shown in Fig. 2 for flame E3 with white circle. OH images of flames E2 and E3 exhibit more disconnected and patchy OH distributions (island structures) downstream due to the existence of high energetic eddies induced by high Re . This results in the existence of zones without OH as shown in flame E3. It is also observed the sudden appearance and disappearance of OH pockets downstream marked by red circles in flame E3 as an indicative of either out-of-plane advection or auto-ignition of hot unburned gases convected towards these locations. Flame quenching/re-ignition behavior, as one of the flame dynamic features, can be further elucidated from these high-speed OH-PLIF images. These images enabled in determining \bar{C} contours.

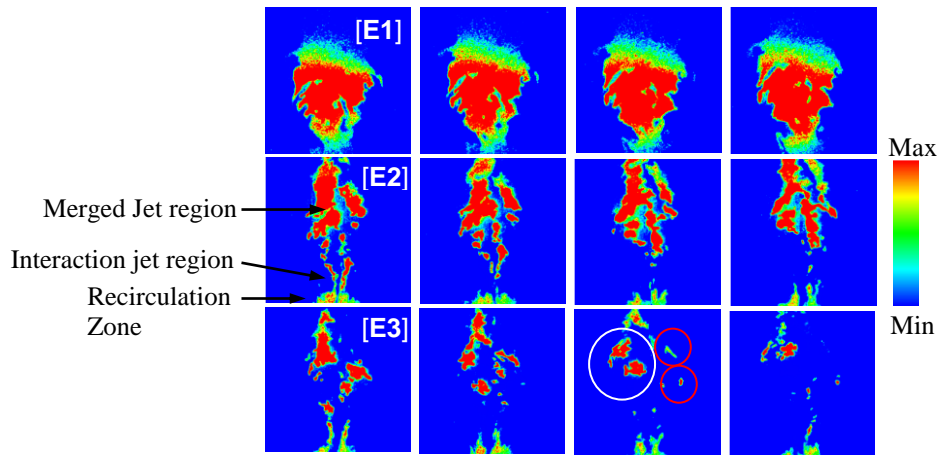


Figure. 2 Sequence of instantaneous OH-PLIF images for flames E1-E3, showing temporal evolution of flame structure, $\Delta t = 0.1$ ms; the bottom line represents the tip of the burner.

3.2 Turbulence and strain rate near blow-off

The extinction of turbulent premixed flames is often described using non-dimensional parameters relating the timescales of chemistry and turbulence, most commonly the Karlovitz number, K , defined by $K = 0.25(u'/u_l)^2(R_l)^{-0.5}$ [9], R_l is the turbulent Reynolds number, $R_l = u'L/v$. u' is the characteristic turbulent velocity fluctuation, which for a three-dimensional velocity field is defined by

$$u' = \sqrt{(u_z'^2 + u_r'^2 + u_y'^2)/3}. \quad u_z', u_r' \text{ and } u_y' \text{ are the RMS velocity fluctuations in the axial, radial and tangential directions respectively. } u_l \text{ is the unstretched laminar burning velocity and } L \text{ is the integral length scale of the turbulence and was evaluated using a two-point correlation of the axial turbulent velocity fluctuation, } u_z'. v \text{ is the kinematic viscosity estimated at the adiabatic flame temperature. Values of } u' \text{ and } L \text{ evaluated along the normalized path length, } S, \text{ of } \bar{C} = 0.05 \text{ and } 0.5 \text{ contours for flames E1-E3 are presented in Fig. 3a and 3c respectively. } S=0 \text{ is defined at } Z=12 \text{ mm for each } \bar{C} \text{ contour, increasing downstream. Values of } u' \text{ and } L \text{ show significant variation along } \bar{C} = 0.05 \text{ contour which becomes trivial along } \bar{C} = 0.5 \text{ resulting from the coincident of shear layers with } \bar{C} = 0.05 \text{ contour. Values of } u' \text{ increase with } Re, \text{ however, } L \text{ seems to be independent of } Re.$$

The local quantification of u' and L from the analysis of the PIV data enables the calculation of the local K along \bar{C} contours of flames E1-E3. Figures 3b and 3d show the variation of K for flames E1-E3 plotted along the normalized path length, S , for $\bar{C} = 0.05$ and 0.5 line contours respectively. Values of K reveal substantial dependency on the position of $\bar{C} = 0.05$; such dependency is insignificant for $\bar{C} = 0.5$. These flames show high values of K upstream, decreasing downstream then increasing again further downstream particularly for flame E3. The axial variation of K is shown in Fig. 4 indicating

high values of K within the recirculation zone and interaction jet region. The localized extinction occurred at the interaction jet region as shown in Fig. 2 is attributed to such high values of K .

Local quenching is likely due to the high flow strain rate exerted on the flame surface. In this regard, the extensive (S_{ext}) and compressive (S_{com}) principal strain rates along the flame fronts are analyzed, which are calculated based on [10]. The probability density function (pdf) of the principal strain rates normalized with (δ_l/u_l) is shown in Fig. 5. The shape of the curve is reasonably Gaussian and S_{ext} (S_{com}) has mostly positive (negative) values, this being consistent with previous data [11]. The ranges of S_{ext} and S_{com} increase as Re increases in flames E1-E3 as indicated by the broadening of pdfs and the shift of the peak probability peaks to larger S_{ext} and S_{com} (see Fig. 5). Values of pdfs in flame E3 reduce as an indication of the increase of the likelihood of the local extinction.

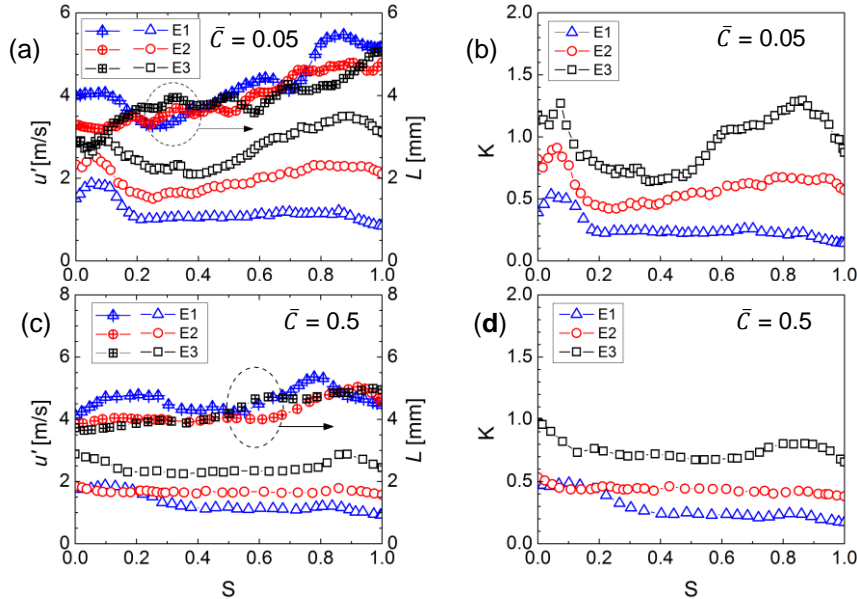


Figure. 3 Variation of u' and L (a,c) and K (b,d) along $\bar{C} = 0.05$ and 0.5 contours for flames E1-E3.

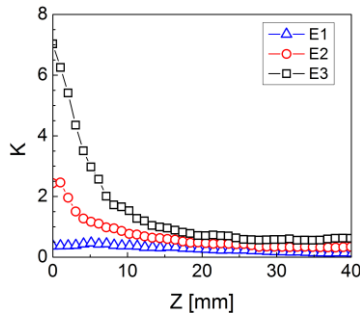


Figure. 4 Variation of K along axial plane for flames E1-E3.

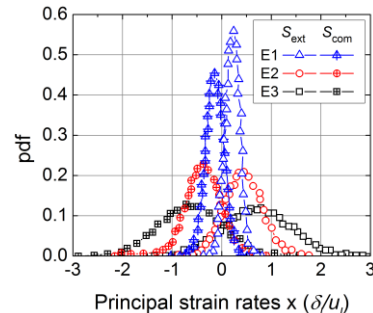


Figure. 5 PDF of normalized principal strain rates along flame front for flames E1-E3.

3.3 Effect of recirculation zone size and hydrogen addition on Blow-off

The concave size has a remarkable influence on the blow-off dynamics in CWJ burner. As this size increases from 16 to 28 mm, the blow-off events are unlikely as shown in Fig. 6a and 6b. As the RZ increases, the local extinction at the interaction jet region reduces. Hydrogen addition effect on the local extinction is pronounced as shown in Fig. 6c and 6d. Even though the flow rate of reactants is kept constant, 10% addition of H_2 reduces such localized extinction. Such trends are not pronounced at higher equivalence ratios.

Once the blow-off event has started, OH measurements at different axial locations (Not shown) indicate that most of the upstream flame regions (IJ region) are destroyed during the approach to blowoff as the anchoring flame regions also experience higher rates of strain and curvature. However, as unburned gases move further downstream, such rates become smaller and flame fronts propagate

normally. As Re increases (flame E3), flames become shorter and are entrained by larger volume of cold reactants. The increased strain rates coupled with heat loss effects result in further fragmentation of the flame, eventually leading to the complete quenching of flames. In this regard, for flames of high Markstien number (Ma), strain alone can cause extinction, whereas flames having $Ma < 0$ require heat loss for extinction to occur [12]. Hydrogen addition decreases Ma but increases burning rate resulting in low probability of localized extinctions.

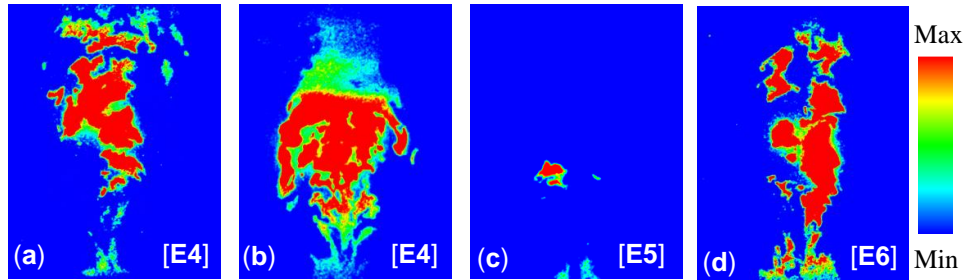


Figure. 6 Snap shots of OH image for flames E4 ($W=16$ mm), E4 ($W=28$ mm), E5 and E6.

4 Conclusions

In this study, high speed OH-PLIF and simultaneous SPIV have been utilized to investigate the blowoff mechanism in curved-wall jet stabilized turbulent premixed flames. The sequence of events leading to blowoff of ethylene-air flames was investigated. Influences of the recirculation zone size as well as the hydrogen addition were scrutinized. Flames, far from blowoff conditions, are characterized with a recirculation zone (RZ) upstream for flame stabilization followed by an intense turbulent interaction jet (IJ) and merged-jet regions downstream. The flame front is highly influenced by the shear layer vortices for low Re flames as wrinkling of the flame front along the shear layer is more pronounced. However, these shear layers are randomly distributed for higher Re flames indicated by the islands of OH pockets. As Re increases, cold reactant penetration to IJ region is significant under high strain rates conditions, which increases the frequency of flame front extinction. The localized flame extinction depends upon the local turbulent Karlovitz stretch factor as well as the cooling of the RZ. The larger the recirculation zone, the less propensity of the local flame extinction. Similar results were found as 10% H_2 was burned with the reactants.

References

- [1] Dally BB et al. (1998). Instantaneous and mean compositional structure of bluff-body stabilized nonpremixed flames. *Combust. Flame*. 114: 119.
- [2] Masri AR et al. (2004). The compositional structure of swirl-stabilised turbulent nonpremixed flames. *Combust. Flame*. 137: 1.
- [3] Bonaldo A, Kelman J B. (2009). Experimental annular stratified flames characterisation stabilised by weak swirl. *Combust. Flame*. 156: 750.
- [4] Gil YS et al. (1998). Premixed flame stabilization in an axisymmetric curved-wall jet. *Combust. Flame*. 113: 348.
- [5] Gregory-Smith DG Hawkins MJ. (1991). The development of an axisymmetric curved turbulent wall jet. *Int. J. Heat and Fluid Flow*. 12: 323.
- [6] Kim D et al. (2009). Characteristics of premixed flames stabilized in an axisymmetric curved-wall jet burner with tip modification. *Combust. Sci. and Tech*. 181: 1397.
- [7] Longwell JP. (1953). *Proc. Combust. Inst.* 4: 90. 13.
- [8] Morley C. Gaseq chemical equilibrium program available at: c.morley@ukgateway.net

- [9] Bradley D. et al. (2005). Premixed flamelet modelling: Factors influencing the turbulent heat release rate source term and the turbulent burning velocity. *Combust. Flame.* 143: 227.
- [10] Han D and Mungal MG. (2003). Simultaneous measurements of velocity and CH distributions. Part 1: jet flames in co-flow. *Combust. Flame.* 132: 565.
- [11] Hartung G et al. (2008). Effect of heat release on turbulence and scalar-turbulence interaction in premixed combustion *Phys. Fluids* 20: 035110.
- [12] Law CK. (1989). Dynamics of stretched flames. *Proc. Combust. Inst.* 22:1381.